Graphene as a pre-illumination cooling approach for a concentrator photovoltaic (CPV) system

Mussad M. Alzahrani [1,2*], Anurag Roy[1], Katie Shanks[1], Senthilarasu Sundaram[1], Tapas K. Mallick [1]

[1]Environmental and Sustainability Institute, University of Exeter, Penryn Campus, Cornwall TR10 9FE, U.K.

[2]Mechanical and Energy Engineering Department, Imam Abdulrahman Bin Faisal University, Dammam, 34212, Saudi Arabia

*Corresponding author: ma778@exeter.ac.uk

A B S T R A C T

The concentrator photovoltaic (CPV) system has a high potential in increasing the power output, propelling further the concentration ratio generating excessive heat that significantly deteriorates the solar cell efficiency and reliability. To thoroughly exploit graphene as a pre-illumination cooling technique for a solar cell, we experimentally characterized screen printed graphene coating (GC) physicochemical characterizations to observe the attenuation of light across a wide wavelength range with different GC thicknesses on a low iron-glass. The thermal and electrical characterizations were further executed to observe the performance of GC on a concentrated CPV system. Based on these comprehensive experimental characterizations, the concept of utilizing graphene as a neutral density (ND) filter for focal spot CPV system is shown to reduce the device temperature significantly by 20% and 12% for $GC_{6.3}$ (6.3µm thickness) and $GC_{2.2}$ (2.2µm thickness) in comparison with the infrared filter, respectively. It has been observed that $GC_{6.3}$ increased the cell efficiency by about 12% at 8suns compared to the base case at 400W/m^2 producing 7suns. It has been ascertained that the introduction of graphene as the ND filter component improved the solar

cell efficiency instead of just reducing the geometrical concentration ratio. Further, even the most susceptible single-junction solar cell under a concentration ratio of ≈ 20suns with no cooling aid has shown an excellent cell efficiency. Therefore, our approach envisages its application for non-CPV and high and ultrahigh CPV system incorporated with a triple-junction solar cell eliminate the use of external heat sinks or other cooling arrangements.

Graphical abstract

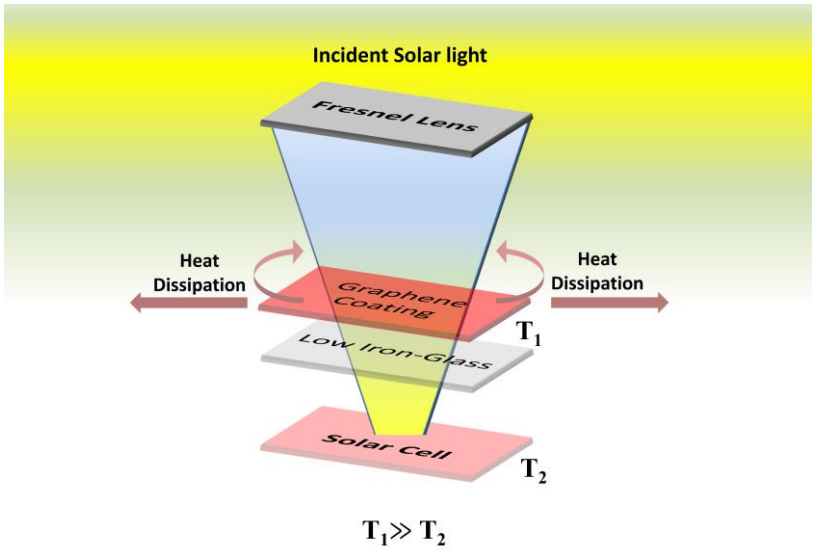

Keywords: graphene, single-junction solar cell, passive cooling, neutral density filter, optical density, Concentrator Photovoltaic.

1. Introduction

The function of the construction of a single junction solar cell is to convert radiation into direct electrical energy. The main issue with the photovoltaic (PV) cell is the energy of the bandgap, in which the photon energy must be greater than the energy of the bandgap to induce the photogeneration of charge carrier. The maximum theoretical conversion efficiency under one sun AM1.5 for a single-junction solar cell is described by Shockley and Queasier to not exceed 33.7% [1], where currently single-junction silicon-based solar cell proposes efficiency of 26.1% and 27.4% [2] for concentrated and non-concentrated solar irradiance, respectively.

The limitation of a single-junction solar cell in absorbing all the incident ray on the PV cell leads to intrinsic thermalization losses which is the cause of heat generation[3]. At 1sun, the outdoor operating temperature of a single-junction solar cell is typically around 55°C:[4–6] where increasing the concentration ratio might raise the thermal impact on the solar cell to be fatal (1200°C) at 400suns [7] with no cooling aid. This amount of heat harms the quality of generated electrical power and the durability of the cell [8,9]. The use of cooling techniques can offer a potential solution to avoid excessive heating of PV panels and to reduce cell temperature [10]. It can be inferred that both air and water cooling methods have been used to a large extent since they can provide additional thermal energy that can be used for different purposes.

Post-illumination or pre-illumination heat extraction techniques are essential to maintain the solar cell performance and reliability for safe operation, especially toward high and ultrahigh concentration ratio. Post-illumination is the conventional solar cell cooling mechanism, including passive cooling and active cooling, which are mainly based on the engineering design concepts and heat transfer components: conduction, convection, and radiation [11]. In a passive cooling approach, a variety of heatsink dimensional configurations[12] are attempting to maintain the solar cell at safe operating conditions for a multi-junction solar cells (MJSCs)[13–17] which can be vulnerable to such high temperatures than single-junction silicon-based cells. On the contrary, active cooling has proven its competence in solar cell thermal management at the cost of a parasitic load especially by increasing the concentration ratio adding to the required load, the system complexity, and the overall system cost[18–22]. In pre-illumination, spectral decomposition[23,24] -including ultraviolet (UV), visible (VIS), and near-infrared (NIR) - for the solar spectrum tolerates bandpass and bandstop. These pre-illuminations mechanisms can lead to high cell conversion efficiencies bypassing the compatible photon energy to the PV cell and redirecting the photon

energy with energy more than the bandgap energy to reduce the cell temperature. Unique configurations including spectral beam splitting (SBS)[25], hot/or cold mirrors[26], holographic optics[27], and luminescent concentrator beam[28], have been mainly focusing on improving the cell efficiency relying on the required load of generation. This spatial pre-illumination approach represents high efficiency in low concentration ratio applications, but it becomes a very complex approach with a high concentration ratio due to the tracking system.

A clear area, where further improvements can be realized, is in the use of selective absorber coatings. Currently, available coating materials are still expensive, subject to degradation and not as efficient as their potential suggests [29–32]. Therefore, the development of sunlight absorbers with rational structure designs has become a popular research topic, because it has remarkable potential to improve efficiency. With a relatively simple generation process and enhanced optical absorption, carbon-based materials have low cost, reusability, and excellent light to heat conversion properties. The combination of maximum light absorption, high specific surface area, and greater thermal stability makes the carbon an effective solar heat absorber material. Graphene exhibits distinct differences from the other carbon nanomaterials in terms of its two-dimensional (2D) features which offers a wide range of interesting properties such as high charge mobilities, superior thermal conductivity, a high degree of transparency, as well as mechanical flexibility among other carbon allotropes.[33,34] Due to its flat elasectronic 2D band structure, it imparts an exceptional horizontal heat conductor with high thermal stability compared to conventional solar absorber coatings. This is due to the existence of the large aromatic network and extent of pi bond cloud which captures the electrons or ions during the diffusion and oxidation process; resulting in a broad Brillouin zone of band structure for the graphene [35–37]. Graphene absorbs and scatters photons at the upper band, and then a part of photons are transmitted to be incident on the solar cell, as schematically represented in Fig. 1. The high absorption capacity of graphene catalyzes strong

interaction between the electronic band of the graphene and incident sunlight results in a strong releasing of heat. A larger portion of the generated heat on the graphene surface is dissipated horizontally. For instance, graphene benefits from the high *in-plane* thermal conductivity, up to a certain channel length. However, weak thermal properties for the substrates implies that interfaces and contacts remain the significant dissipation bottlenecks. The heat generation mainly originates from the phonon-phonon coupling within the graphene electronic band structure [38,39].

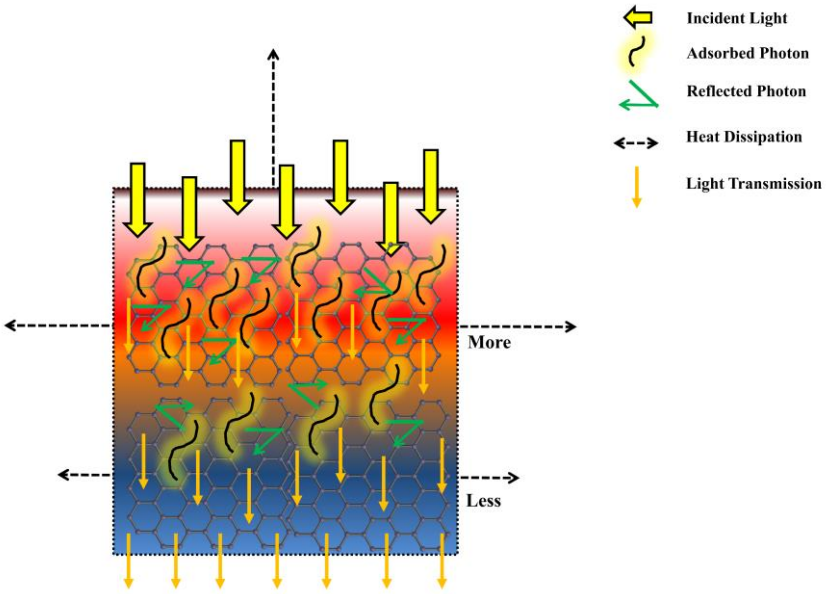

Fig. 1 Scheme of localized solar heating and light transmission of the graphene coating

The concentrator photovoltaic system has a high potential for encouraging power output and reducing the cell size [40–42]. The progression of concentrated photovoltaic (CPV) configuration inclines to increase the concentration ratio and upsurge the competitiveness in the CPV system. This increment in concentration ratio results in minimizing the MJSC cost contribution to the overall system cost [43]. Although the increase of concentration ratio on the MJSC would produce more power despite their low efficiency beyond 1000suns, the expensive low internal resistance MJSC cannot overrun a temperature of 110°C [44]. Indeed, this

temperature influence will be excessive for single-junction solar cells. In order to address this issue, a neutral density (ND) filter is fabricated utilizing a graphene material to attenuate the transmittance of solar irradiance over a wide spectral band. The optical density (OD) of graphene material from colourless to dark in appearance regulates the amount of energy incident on the cell at which heat generated on the solar cell is controllable in inverse correlation with optical density. More recently, the concept of infrared (IR) filter [45,46] or heat-absorbing filters[47] has evolved into a photonic approach to perform a radiative cooling technique selectively exploiting sunlight with consideration for bandgap energy but with a reduction in cell temperature by 5.7°C [48]. Coinage metals, such as gold, silver, copper exhibits a high reflectance at the (NIR)[49] and are commonly utilized in ND filter. The standard method to fabricate a ND filter is by coating glass with a thin layer of materials with possessing a different material, such as Co, Fe, and Cr, with precise control of the alloy composition through a vacuum procedure [50–52].

Since the electrical products for the solar cell rely on the solar irradiance intensity, solar cell temperature, and the wavelength band, the influence of diverse colure filter was found in the literature [53]. Indeed, the PV module is influenced under a selective band of wavelength, and excellent performance was found for both blue and magenta. However, the highest electrical performance was found by subjecting all the wavelength band (no filter) on the PV module, and that can be attributed to the actuality of receiving the maximum solar irradiance in the lack of any filters. Besides that, the PV module temperature with no filters was not the maximum one in comparison to all sorts of coloured filters [54]. The utilization of coloured filter has undoubtedly resulted in the cut-off of light intensity intrinsic to the tint of the filter. Thus, in this study, graphene is used as a neutral density filter to attenuate the entire incident solar irradiance by uncomplicated characterization method (no power).

The integration of graphene in the CPV system specifically at the top of the front-grid metallization of triple junction III-V solar cells is studied for one graphene monolayer or two graphene monolayers. The utilization of graphene as a transparent electrode allows the series resistance mitigation. The simple concept is that one monolayer of graphene absorbs lights, causing a reduction of 1% in the change of the short circuit current (ΔIsc). However, in return, the excellent electrical conductivity of graphene provides significant gain by the change of fill factor (ΔFF) $\approx 2\%$ at a concentration ratio of 1000suns [55,56]. The incorporation of graphene one monolayer has shown a drop in the solar cell series resistance by 35% and improve the FF by 4% at 1000suns where two monolayer reduced the series resistance but did not increase the FF due to the optical loss [56]. Further study has integrated one monolayer of graphene between the front-grid and the antireflective coating and compare its energy gain result with conventional III-V solar cell at 800suns. The energy gain increased between 6-7% based on the geographical location when using the monolayer of graphene [57].

The ongoing research in fabricating and developing a CPV system is to achieve a high optical concentration ratio for higher electrical power output, maintaining an excellent solar cell efficiency. The concept for high electrical output is through attaining as much as possible of the geometrical concentration ratio, and that only occurs when the CPV system has high optical efficiency. However, practically the optical efficiency is compromised electrically depending on the solar cell electrical performance where attention needs to be paid to the amount of concentrated light(generated temperature) on the surface of the solar cell to avert the increase in the solar cell electrical series-resistance. It is a possible solution to reduce the temperature elevation by reducing the geometrical concentration ratio, but this approach is not toward the advances in CPV technology [58]. Differently, allowing CPV system advances is through a high level of geometrical concentration ratio giving a range of optical losses at which higher power output is produced by associating a suitable cooling mechanism. Although using

graphene as a neutral density filter causes an optical loss across the wavelength range evenly, the excellent opto-thermal properties of graphene compensate the system by reducing the focal spot temperature at which a higher cell efficiency is gained.

Many studies have investigated graphene based on single or multijunction deposited on the front-grid of the solar cell but none of which has examined graphene as a pre-illumination method (ND filter) coupled in a CPV system based on Fresnel lens design and its power output potential. The fabrication of graphene as an ND filter will aid the advances and evolution of CPV systems to reach a high concentration ratio by limiting the cell temperature which allows the thermal-mechanical effect to be decreased, the electrical performance to be enhanced, the utilization of low cost and high series resistance solar cells, the employment of continuous 3-D tracking system in pre-illumination cooling techniques, and the minimization of overall system weight, cost, and parasitic load by cancelling the post-illumination cooling mechanism. To illustrate the efficacy technique, in this study four approaches have been conducted for full characterization and analyzation of Graphene ND filter utilization in CPV system; chemical characterization, optical characterization, thermal characterization, and electrical characterization.

2. Experimental Approach Description

2.1. Preparation of graphene coating and optical characterization

The chemical characterization of the graphene coating (GC) is executed by using the graphene ink (Product No. 900960), Sigma Aldrich, and used without any further purification. A layer of graphene ink is employed to develop the coating on a $5 \times 5 cm^2$ low iron-glass (4mm thick) by a screen-printing (120T mesh/inch, Mascoprint, UK) method. The low iron-glass with an excellent performance in both visible and NIR wavelength range has been used for the deposition of graphene quantity and optical characterization, as in Fig. 2a. The low-iron glass-

coated samples were characterized based on graphene quantity: thick, medium, and thin coatings, as in Fig. 2c. After each layer of deposition, the sample has been heated for a 120°C for 10minutes and allowed to cool for next layer deposition. Finally, the prepared coating is then heated on a hot plate at 300°C for 30minutes to remove the binders.

The total transmittance of low iron-glass, different GCs on low iron-glass and the IR filter (Fig. 2b) was measured using a PerkinElmer LAMBDA 1050+ UV/Vis/NIR spectrophotometer in a spectral range of 300 –2000nm for optical characterization and comparison among the coated samples and with the IR filter.

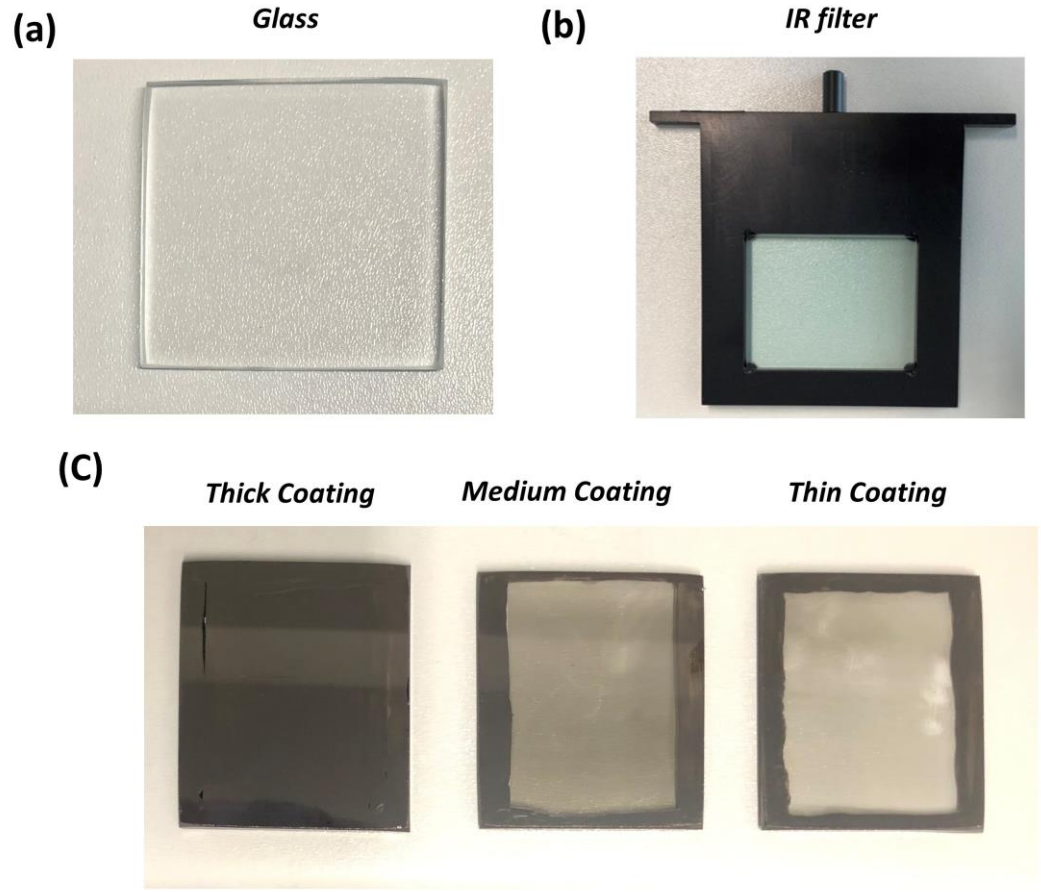

Fig. 2 (a) the digital image of the low iron-glass. (b) the photo of IR filter. (c) the digital image of different samples of GC classified based on the graphene quantity on the glass.

2.2. Thermal and electrical characterization of graphene coating

To perform the thermal and electrical characterizations, a WACOM AAA rating and 2% spatial non-uniformity was applied. Xenon short-arc lamp plus and optical filter are combined to simulate a continuous solar irradiance at AM1.5 spectrum coincidence. The provided calibration cell with the WACOM solar simulator was used to ensure the strong linear correlation between the I_{sc} and the helicon value (solar irradiance) with the attenuation of the Xenon lamp intensity and the consistency of the solar irradiance.

A refractive [Silicon-on-glass (SOG) - Fresnel lens] optic of 529cm^2 (23cm × 23cm) area was introduced under the solar simulator (WACOM) at a constant solar irradiance of 1000W/m^2 and adjusted in elevation for the optimum focal spot and focal length where the highest concentration ratio was achieved. A polycrystalline Si solar cell of 26cm^2 (5.1cm × 5.1cm) area was placed within the focal spot and centred for maximum electrical output. A polycrystalline Si solar cell was soldered with a tabbing wire (electrical terminal) applying a solder flux along the cell's busbar for oxidization and soldering tip at a temperature of 350°C. The electrical terminals are connected to the I-V tracer device to extrapolate the electrical products with time intervals. The experimental setup to concentrate the solar irradiance using the Fresnel lens results in a geometrical concentration ratio of ≈ 20suns at a focal spot of ≈ $3cm$ in diameter and a focal length of ≈ 44cm. The gap between the polycrystalline Si solar cells and the low iron-glass is kept ≈ 4cm because direct contact with the polycrystalline Si solar cells, where the focal spot temperature is significantly high, induces the thermo-mechanical effects and hinders the FF, as schematically and experimentally layout in Fig. 3a and b.

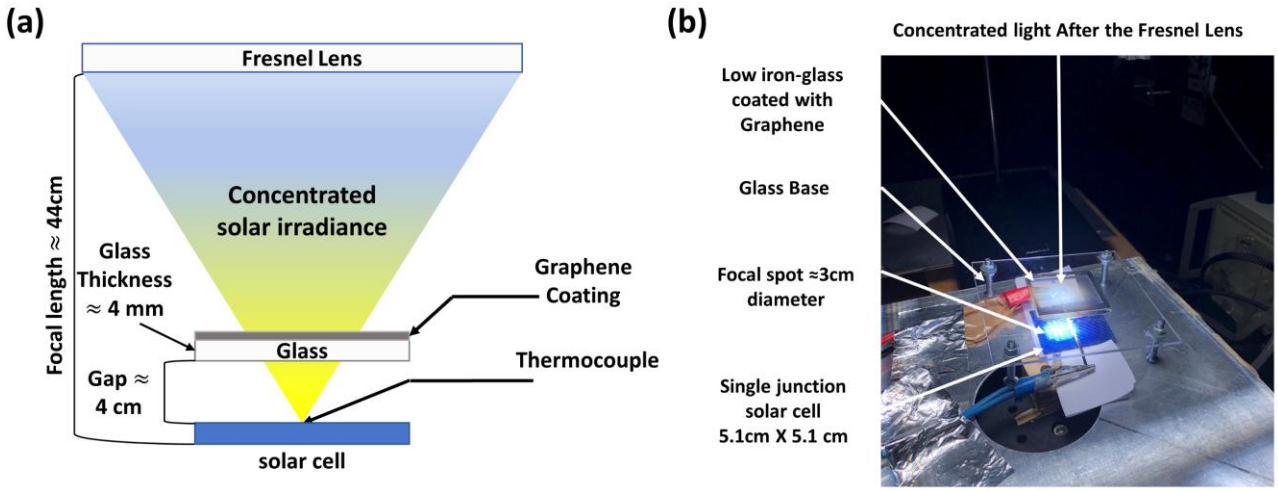

Fig. 3 (a) the schematic approach to generate concentration and measure the focal spot temperature and layout the gap between the solar cell and low iron-glass. (b) the experimental approach under the solar simulator indoor.

For thermal characterization, the temperature is measured and collected utilizing a thermocouple meter (Datalogger SDL200 - EXTECH INSTRUMENTS). As well, the FLIR thermal camera is utilized to observe the thermal distribution across the area of the focal spot and the low iron-glass coated with graphene.

3. Results and Discussion

3.1. Chemical characterization

The cross-sectional microstructural scanning electron microscope (SEM) image of the GC samples were analysed on a TESCAN VEGA3 SEM. Different coating thicknesses of the graphene sample on low iron-glass is achieved by a number of screen-printed layers of graphene ink, as in Fig. 4. In this case, using one layer of graphene screen printing coating resulted in an average thickness of 2.2 ± 0.2µm, which is termed as a thin coating ($GC_{2.2}$), as in Fig. 4a. Further, two and three layers of graphene ink are used to fabricate an average thickness of 6.3 ± 0.1 and 9.1 ± 0.05µm of coating and termed as medium ($GC_{6.3}$) and thick

coating ($GC_{9.1}$), as in Fig. 4b and c, respectively. These three different thickness-based GCs are further employed for further characterizations.

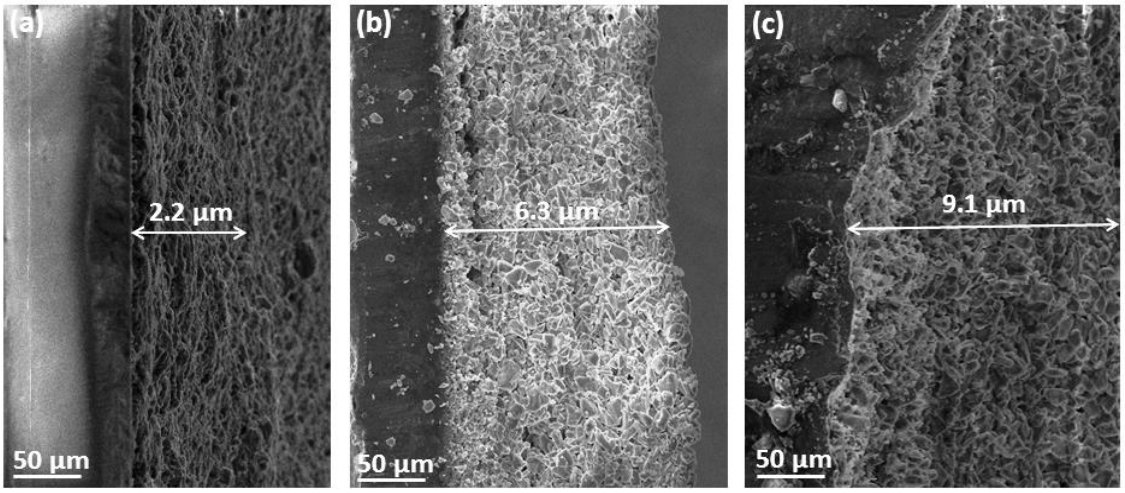

Fig. 4. cross-sectional SEM images of (a) one ($GC_{2.2}$), (b) two ($GC_{6.3}$) and (c) three ($GC_{9.1}$) layer of screen-printed GC using graphene ink on glass, respectively.

3.2. Optical characterization

Graphene is optically characterized to comprehend its optical performance as an ND filter and compared with the most common photonic approach IR filter approach in a wide spectral range of 300 – 2000nm. In this study, the CPV unit is based on a Fresnel lens design where the optical performance of all optics and filters integrated after is dependent on the optical behaviour of the Fresnel lens. Thus, the measurement for the total transmittance of the Fresnel lens has found to be 90%. The total transmittance of the low iron-glass has an average loss of ≈11% after the graphene has been coated on top of it to attenuate the transmittance of the solar spectrum. The attenuation of solar irradiance has been approached by differing the thickness of graphene during the coating process resulting in $GC_{9.1}$, $GC_{6.3}$, and $GC_{2.2}$ after the chemical characterization. The optical characterization of $GC_{9.1}$, $GC_{6.3}$, and $GC_{2.2}$ shows an average total transmittance of 2%, 43%, and 64 %, respectively. As well, the total transmittance of the IR filter has an average of 74% in a wavelength range of 300-700nm where after all

spectral wavelength is blocked to mitigate the heat. However, considering a wide spectral range of 300 – 2000nm results in IR filter average transmittance of 19%. The optical measurements for the IR filter are conducted to compare its performance with GCs. The thickness of the GC has an inverse correlation with the transmittance of light.

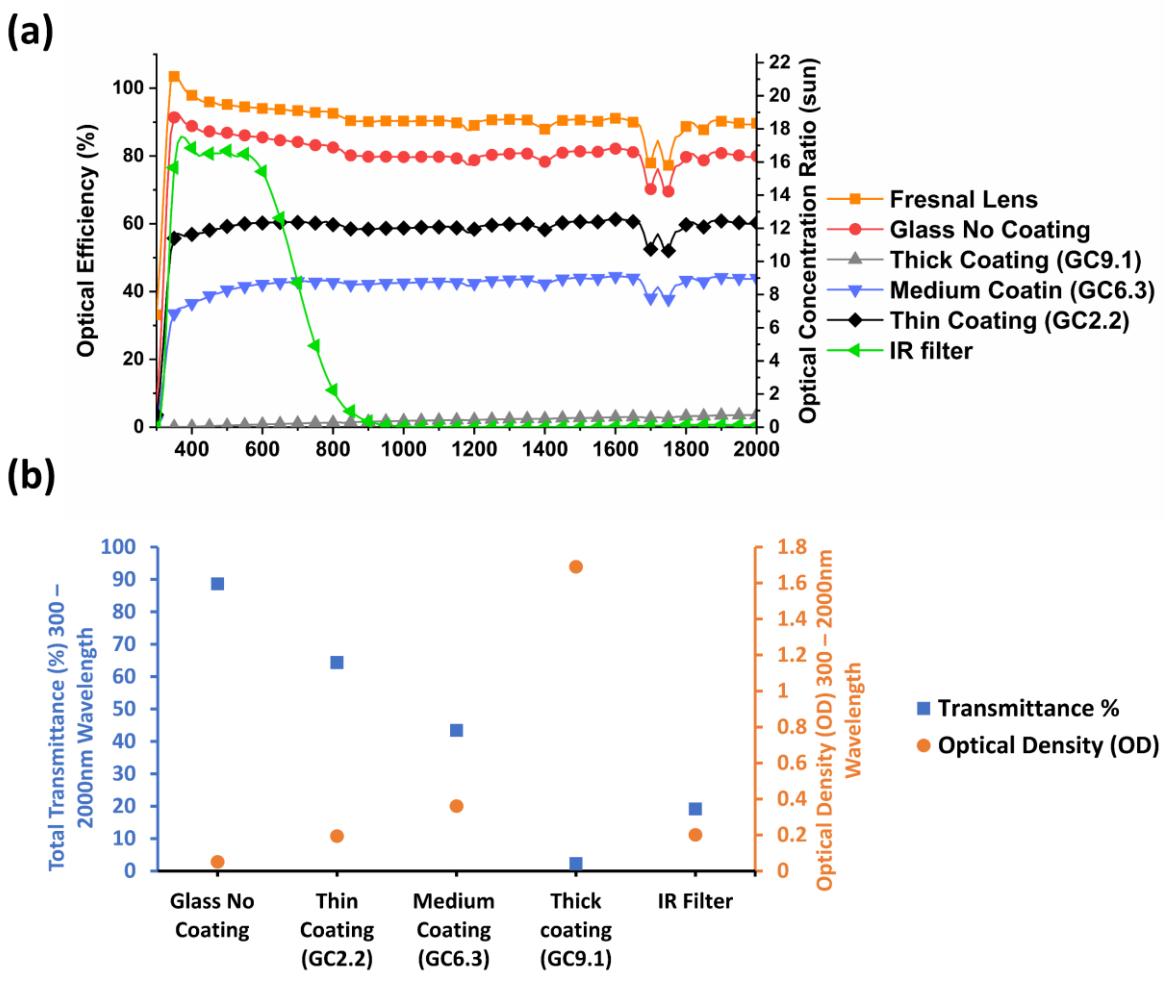

Fig. 5 (a) the correlation between the optical efficiency and the optical concentration ratio for Fresnel lens, IR filter, low iron- glass, $GC_{9.1}$ coating, $GC_{6.3}$ coating, and $GC_{2.2}$ coating with a wavelength range between 300–2000nm. (b) the total transmittance and the optical density (OD) for the Fresnel lens, IR filter, low iron-glass, $GC_{9.1}$ coating, $GC_{6.3}$ coating, and $GC_{2.2}$ coating.

To illustrate, the optical characterization, optical efficiency and concentration ratio need to be investigated to see the deterioration in the optical performance with the Fresnel lens at first and then with integrating the IR filter, low-iron glass, $GC_{9.1}$, $GC_{6.3}$ and $GC_{2.2}$ in one CPV unit, respectively. The incorporation of the optical efficiency of the Fresnel lens ($\eta_{Fresnel}$), IR filter ($\eta_{IR_{Filter}}$), low-iron glass (η_{glass}), and low-iron glass with GC_s (η_{GC_s}) results in the total theoretical optical efficiency for the CPV unit, which is a relevance between the concentrated solar irradiance passing all-optical stages with respect to the incoming solar irradiance at the primary optical stage surface area, as in the equation 1

$$Optical\ Efficiency = \eta_{Fresnel} \times \eta_{IR_{filter},\ glass,\ GC_s} \quad (1)$$

The calculated optical efficiency is substituted in equation (2) to extrapolate the optical concentration ratio.

$$Optical\ Concentration\ Ratio = Optical\ Efficiency \times G_C \quad (2)$$

where G_C is the geometrical concentration ratio which is the area of the Fresnel to the area of the solar cell.

As in Fig. 5a , the optical efficiency and concentration ratio are measured for after the Fresnel lens and with every test scenario at every wavelength unit. As on average for a wavelength range of 300–2000nm, the optical efficiency after the Fresnel lens is 90% and equivalent to the optical concentration ratio of 18suns and with integrating the low-iron glass the optical efficiency and concentration ratio dropped to 80% and 16suns, respectively. The graphene coatings dropped the optical efficiency from after the Fresnel to 2%, 42%, and 58% and the optical concentration ratio from after the Fresnel to 1sun, 8suns, and 12suns for $GC_{9.1}$, $GC_{6.3}$, and $GC_{2.2}$, respectively. The IR filter showed a drop from after the Fresnel to 18% and 4suns for the optical efficiency and concentration ratio, respectively. The total transmittance of

GCs has shown almost no fluctuation across the measured wavelength length, indicating less dispersion of light and that is due to the high absorptivity of graphene relative to its thickness. However, Fig. 5a showed that IR filter, low iron- glass, and GCs are dependent on their performance on the primary optic Fresnel lens and that can be observed across the wavelength range.

The measurements of the total transmittance of graphene ND filter allow us to characterize the graphene in terms of optical density (OD) instead of quantity by exploiting the transmittance as the logarithm to the base ten, as in equation 3.

$$Graphene\ Optical\ Density = -log_{10}(\%T_{avg}) \quad (3)$$

Where $\%T_{avg}$ is the average transmittance for a wavelength range between 300–2000nm.

Fig. 5b shows an inverse correlation between the optical density and total transmittance. The ODs are 0.045 0.13, 0.05, 1.69, 0.36, and 0.193 for the Fresnel lens, IR filter, low-iron glass, $GC_{9.1}$, $GC_{6.3}$, and $GC_{2.2}$, respectively. Table 1 summarises the total transmittance on average, optical density (OD), optical efficiency, and optical concentration ratio for the optically characterized samples.

It is crucial to evaluate the current production from the polycrystalline Si solar cell when illuminated by wavelength range similar to polycrystalline Si solar cell spectral response range. In order to execute the spectral response, the external quantum efficiency (EQE) was measured for a wavelength range between 300 – 1100nm using Bentham spectral response arrangement, as shown in Fig. S1, SI. The current density, J_{sc} (mA/cm^2) is determined by uniting all the photon energy with the EQE and integrating cross all the correspondent wavelength range to be 38.26 mA/cm^2.

Tested Samples	Avg. Transmittance (%)	Optical Density (OD)	Optical Efficiency (%)	Optical Concentration ratio (suns)
Fresnel Lens	90	0.045	90	18
IR Filter	19	0.72	18	4
Glass No Coating	89	0.05	80	16
Thick coating ($GC_{9.1}$)	2	1.69	2	1
Medium Coating ($GC_{6.3}$)	43	0.36	42	8
Thin Coating ($GC_{2.2}$)	64	0.193	58	12

Table 1 the optical characterization for the measured total transmittance, calculated optical density, optical efficiency, and the optical concentration ratio

3.3. Thermal characterization

Thermal characterization is conducted to observe the fluctuation of temperature over time for the focal spot produced by the Fresnel lens and then with the introduction of uncoated low iron-glass and with the GCs, as schematically in Fig. 3a. Three thermocouples were attached at the centre of the graphene layer (top surface of the glass facing the Fresnel lens), the centre of the rear glass surface, and the centre of the focal spot. The rear surface of the glass temperature was measured to observe the temperature difference on the glass and identify any cause for thermal shock, as in Fig. 6a. The temperature was recorded in the three positions. The focal spot temperature reaches the saturation (observing no accumulation in temperature) within a short time of 10seconds at which the temperature of the graphene layer was found to be 211.7±4°C for all the GCs samples. It is undoubtedly expected that high accumulation of heat on the graphene layer would occur resulting in severe temperature degrading the graphene layer with time. The back surface of the glass was found to be 107°C, 179°C, and 180°C for $GC_{2.2}$, $GC_{6.3}$, and $GC_{9.3}$, respectively, as in Fig. 6b. As the graphene thickness decreases, the temperature gradient between the graphene layer and rear surfaces of the glass decrease as well. In order to conduct similar temperature measurements, the orientation of the glass has also been altered where the graphene layer was facing the solar cell, as in Fig. 6c. The results exhibit a minimal temperature difference between the graphene layer and the other side of the glass surface, and that is because glass is much heat conductor than air. However, the focal spot temperature, in comparison to the graphene facing the Fresnel lens, increased on average by 1.63%, 8.8%, and 2.2% for $GC_{2.2}$, $GC_{6.3}$, and $GC_{9.3}$, respectively, as in Fig. 6d. This rise in the focal spot temperature is related to the amount of heat accumulated in the graphene layer drives both heat radiation and convection in its surrounding (4cm distance between the solar cell and the graphene layer). Although this temperature gradient is not significant, we kept the orientation of the graphene layer facing the Fresnel lens. The influence of temperature on the

Fresnel lens – SOG is out of the scope of this study; however, enough safe distance of 39.6cm between the graphene layer and Fresnel lens ensures no impact for accumulated heat.

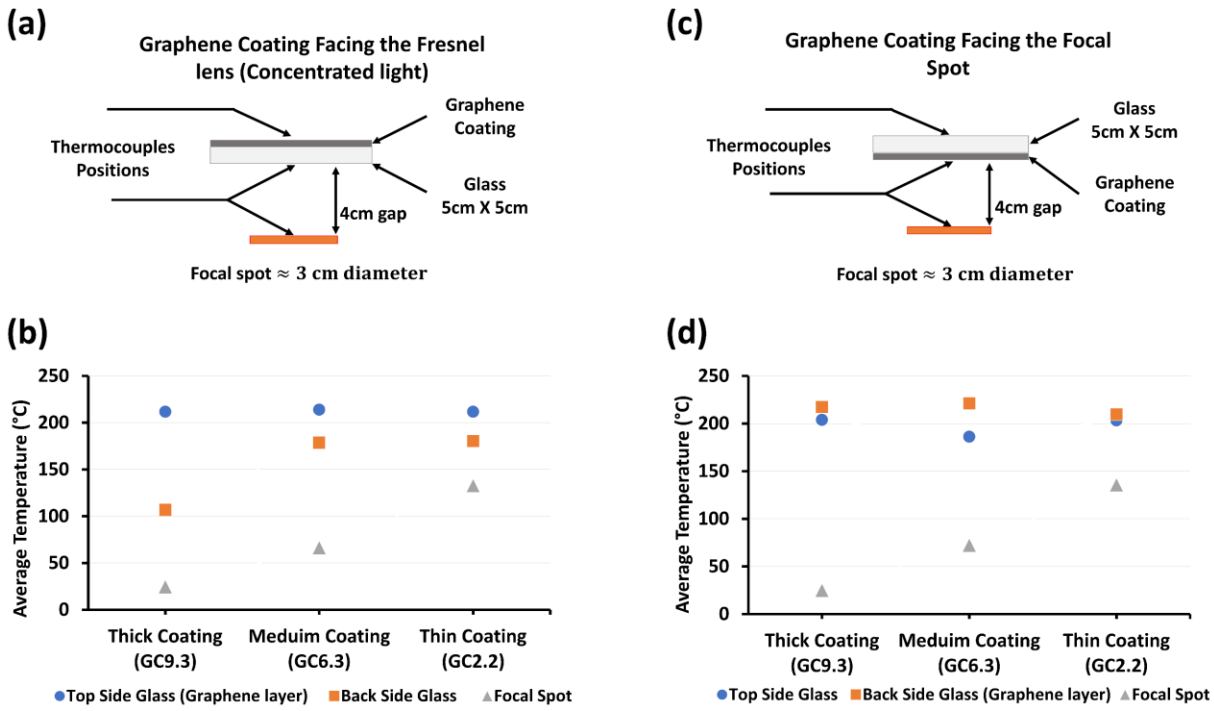

Fig. 6 Thermal investigation for (a) graphene layer facing the Fresnel lens and (c) graphene layer facing the focal spot. The average temperature at the centre for the top side of the glass, the back side of the glass, and the focal spot for (b) graphene layer facing the focal spot and (d) graphene layer facing the focal spot.

Temperature measurements are extrapolated on average after it reaches the equilibrium. Once the solar simulator lamp was on, the temperature reached its saturated level within a maximum of 10seconds and relatively maintained for 70seconds, and when the solar simulator lamp was turned off, the temperature released to the surrounding within 20seconds to reach a room temperature of 22°C, as in Fig. 7a. The introduction of the Fresnel lens has shown a focal spot temperature of 219°C, which after the introduction of the uncoated low iron-glass has attenuated the light slightly reducing the focal spot temperature by 11%. However, the GCs show a significant drop in the focal spot temperature by 89%, 70%, and 39% for $GC_{9.1}$, $GC_{6.3}$,

and $GC_{2.2}$, respectively. The focal spot temperature has an inverse correlation with the optical density due to the effectiveness of graphene as a thermal insulator depending on the graphene thickness and that is observed through the consistency of temperature with time. Thus, the introduction of the graphene ND filter shows an average focal spot temperature of 24.6°C, 66.4°C, and 132.7°C for $GC_{9.1}$, $GC_{6.3,}$ and $GC_{2.2}$ coating measured with the thermocouple, respectively. Fig. 7b shows the correlation between the optical efficiency and the focal spot temperature to illustrate the optical and thermal operating conditions. Fresnel lens and glass no coating have shown the highest optical efficiency but challenged by the highest focal spot temperature. Whereas, it can be observed that the $GC_{6.3}$ and $GC_{2.2}$ have shown that the optical efficiency relatively low in comparison with the Fresnel lens and with uncoated glass but with much reduction in focal spot temperature where the $GC_{9.1}$ has shown the lowest for both focal spot temperature and optical efficiency. The utilization of the IR filter in this experiment is due to its working principle of minimizing heat to the most by cutting off light near IR to ensure excellent electrical performance and to avoid any damage on the solar cell surface. The comparison between the moderate ND filter thermal performance for $GC_{6.3}$ (300 - 2000nm) and the IR filter (300 - 900nm) is expected to exhibit less temperature after the IR filter due to the difference in the wavelength range in accordance to the polycrystalline Si solar cell spectral response (300 – 1100 nm) at which the IR filter has shown an optical efficiency lower than the optical efficiency of $GC_{6.3}$ by 38%. However, the IR filter has shown a focal spot temperature of 117.28°C, which is higher than the focal spot temperature of $GC_{6.3}$ by 43%.

The thermal images were taken for $GC_{6.3}$ to investigate the heat distribution across the top surface. Fig. 7c shows the temperature increasing causing a large area on the top surface of $GC_{6.3}$ with a total testing time of 100seconds where the left thermal image shows the thermal distribution at the initial testing time (~1cm at the centre). The right thermal image shows the thermal distribution where the temperature scale is at least 151°C increase from 1cm to 3cm at

the centre. The saturation in the right thermal image is due because the temperature is chosen as a maximum of 151°C to show how heat is conducted and distributed given the time frame of 100 seconds on the graphene layer. Longer test time might show a uniformed output across the total area of the GCs (greater than the focal spot size), which brings the graphene as a superior thermal conductor material for the thermal applications, and that can be simplified because as graphene holds the thermal conductivity of~ 3000Wm^{-1} K^{-1} [35].

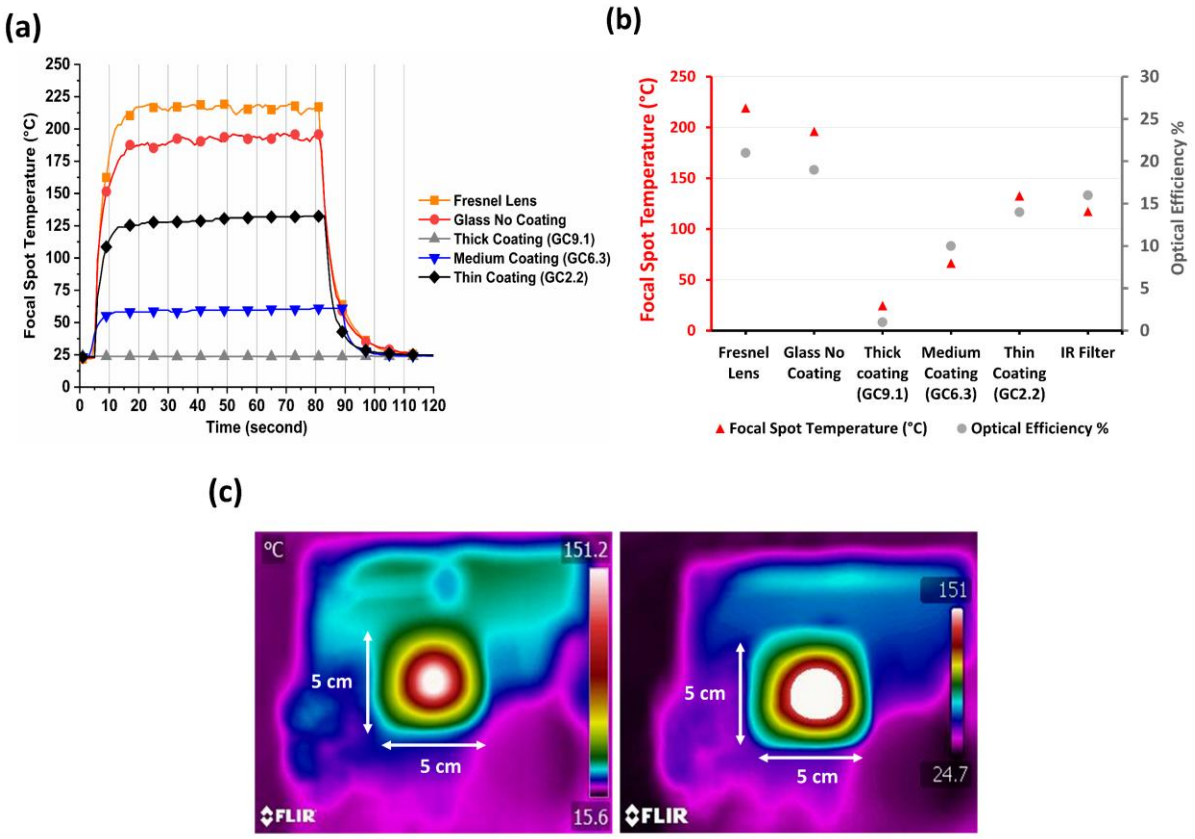

Fig. 7 (a) the focal spot temperature (thermocouple measurement) over time produced by the Fresnel lens and with glass, with $GC_{9.1}$, with $GC_{6.3}$, and with $GC_{2.2}$, respectively. (b) the correlation between the focal spot temperature (thermocouple measurement) and the optical efficiency for the Fresnel lens and with glass, with $GC_{9.1}$, with $GC_{6.3}$, and with $GC_{2.2}$, respectively. (c) the thermal camera image for the $GC_{6.3}$ to show the thermal distribution across the 5 cm x 5 cm area based graphene layer (the temperature scale was set at 151°C).

3.4. Electrical characterization

The polycrystalline Si solar cell electrical products I_{sc}, open-circuit voltage (V_{oc}), and FF, which can be determined simply from the I-V curve, are affected by the increase in the concentration ratio. The large flow of photons increases the current with inducing joule heat on the solar cell surface area. Increasing the concentration ratio (temperature) leads to a reduction in the V_{oc} with significant growth in the I_{sc}. This increase in current density due to the solar concentration inclines to source additional resistive losses in the solar cell beside the losses at its standard design conditions at 1sun where the influence of the resistive loss can be detected by observing the FF (flattening in the squareness shape of the I-V characteristic curve). The impact of series resistance is producing a decrease in the FF and thereby drop in cell efficiency.

Metallization acts an essential role in both optical and electrical performance of the polycrystalline Si solar cell. Optically, where the width of the gridlines associates to shading impacting the I_{sc}. Electrically, through the series resistance of metal conductors impacting the FF. The effect of resistance on polycrystalline Si solar cell is reflected through wasting power in the resistance components. Considering one diode (solar cell) model, the impact of resistance on polycrystalline Si solar cell under no concentration is significant as the temperature increase, and therefore resistance effect exaggerates under a concentration ratio due to the imbalance of the current production to the solar cell area. The utmost common resistances in one diode model is series resistance (R_s) and shunt resistance (R_{sh}). The R_s losses rise substantially due to having a current flow beyond the capacity of the electrical connectors on the solar cell surface area. The R_s is impacted by factors such as semiconductor material resistivity (emitter) and metal conductors (Busbar and fingers). In contrast, the R_{sh} is mainly affected by the impurities adjacent the p-n junction, as in Fig. 8a and b.

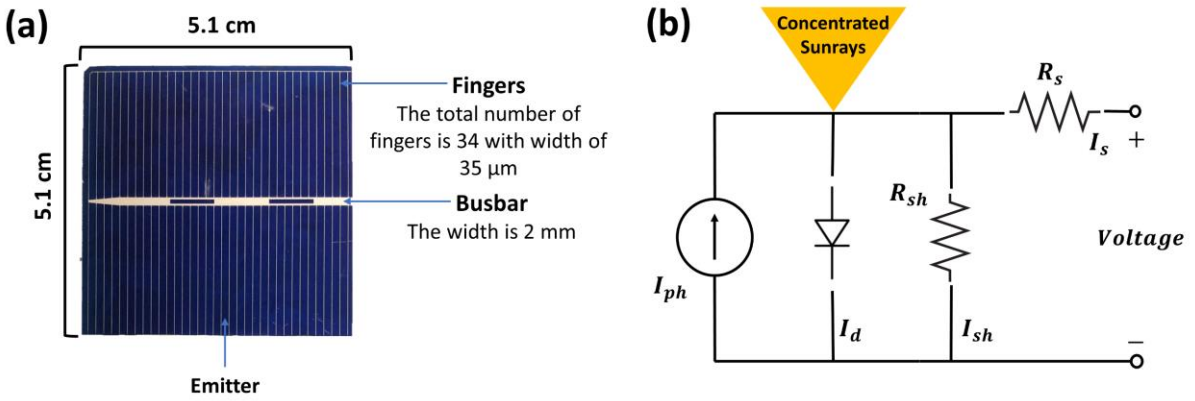

Fig. 8 Illustration of (a) dimensions and series resistance factors and (b) electrical circuit of a solar cell with one diode model, where I_{ph} is the photo-generated current, I_d is the diode current, and I_{sh} is the shunt current [59].

The indoor electrical characterization examines the effectiveness of the graphene ND filter with the high series resistance 5.1cm × 5.1cm polycrystalline Si solar cell (300–1300nm). To observe the fluctuation in performance for comparison and analysis, the electrical components such as I_{sc}, V_{oc}, and FF are measured on the polycrystalline Si solar cell under only the Fresnel lens and after with glass, with $GC_{9.1}$, with $GC_{6.3}$, with $GC_{2.2}$, and with IR filter. Many cells were soldered and prepared for the testing because the polycrystalline Si solar cell is easily cracked under the concentrated solar irradiance due to its low thermal expansion (fragility). The IR filter itself was not enough to avoid the breakage of the polycrystalline Si solar cell. Thus, the IR filter was associated with a cooling mount base set at 25°C to operate the solar cell in a safe condition and also bring the IR filter to the competition with the GCs for comparison.

Although determining the J_{sc} through the EQE is advantageous being independent for the used light source spectral figure, the J_{sc} was carried out also through the I-V curve measurements by illuminating the polycrystalline Si solar cell with solar irradiance of 1000W/m^2 (no concentration) and found to be 37.82mA/cm^2, as shown in Fig. S2, SI. The minimal discrepancy of 1.2% between the EQE calculation and I-V curve measurement is

might be due to either the contact area of the cell being undetermined or the inaccurately of the simulated solar irradiance.

In Fig. 9a, I-V curve shows the dependence of I_{sc} on the illumination and V_{oc} on the temperature where the attenuation of the solar intensity has shown the highest and lowest I_{sc} for the polycrystalline Si solar cell under the Fresnel and $GC_{9.1}$ to be 7510mA and 255mA, respectively. On the other hand, the uppermost and the lowest V_{oc} is for $GC_{6.3}$ and $GC_{9.1}$ to be 631mV and 588.2mV, respectively. The least I_{sc} and V_{oc} for the $GC_{9.1}$ is due to the excessive blockage of light. The apical I_{sc} value for only under the Fresnel is because the optical efficiency of 90%, where the apical V_{oc} value for the $GC_{6.3}$ relies on the accomplished focal spot temperature in comparison to other test scenarios, as in Fig. 9d. Both $GC_{6.3}$ and the IR filter with a cooling mount base has a lower I_{sc} than the $GC_{2.2}$ by 31% and 58% respectively. However, both $GC_{6.3}$ and the IR filter with a cooling mount base has a higher V_{oc} than $GC_{2.2}$ by 2.4% and 0.62%, respectively. Fig. 9b shows the highest maximum power for under the Fresnel (1.5 W), and a similar maximum power of 1.49W for both the glass no coating and $GC_{2.2}$ where glass no coating has a higher I_{sc} than the $GC_{2.2}$ and $GC_{2.2}$ has a higher V_{oc} than glass no coating by 8.8%, respectively. Then after, $GC_{6.3}$ and IR filter with a cooling mount base come with a drop in the maximum power by 11% and 32% in comparison to $GC_{2.2}$, respectively. In case of $GC_{9.1}$, the maximum power is recorded about 0.11W.

In addition, FF has to be investigated with both the optical efficiency and focal spot temperature because the hight intensity of the current flowing via the solar cell causes a resistive loss where its primary influence can be observed through the FF. In Fig. 9c and d, the FF has an inverse correlation with the optical density of graphene and the focal spot temperature. The most influenced FF is the one for the Fresnel lens due to the highest optical efficiency and hence the focal spot temperature. It has been observed that the medium coating exhibited the optimum FF value of 0.446 as a result of the lowest series-resistance reflected on

a relatively less flattening of the solar cell output characteristic with an optical efficiency of 10%, as highlighted in the box in Fig. 9c and d. The observation of the FF is needed to be considered in the consecutive section to find solar cell efficiency.

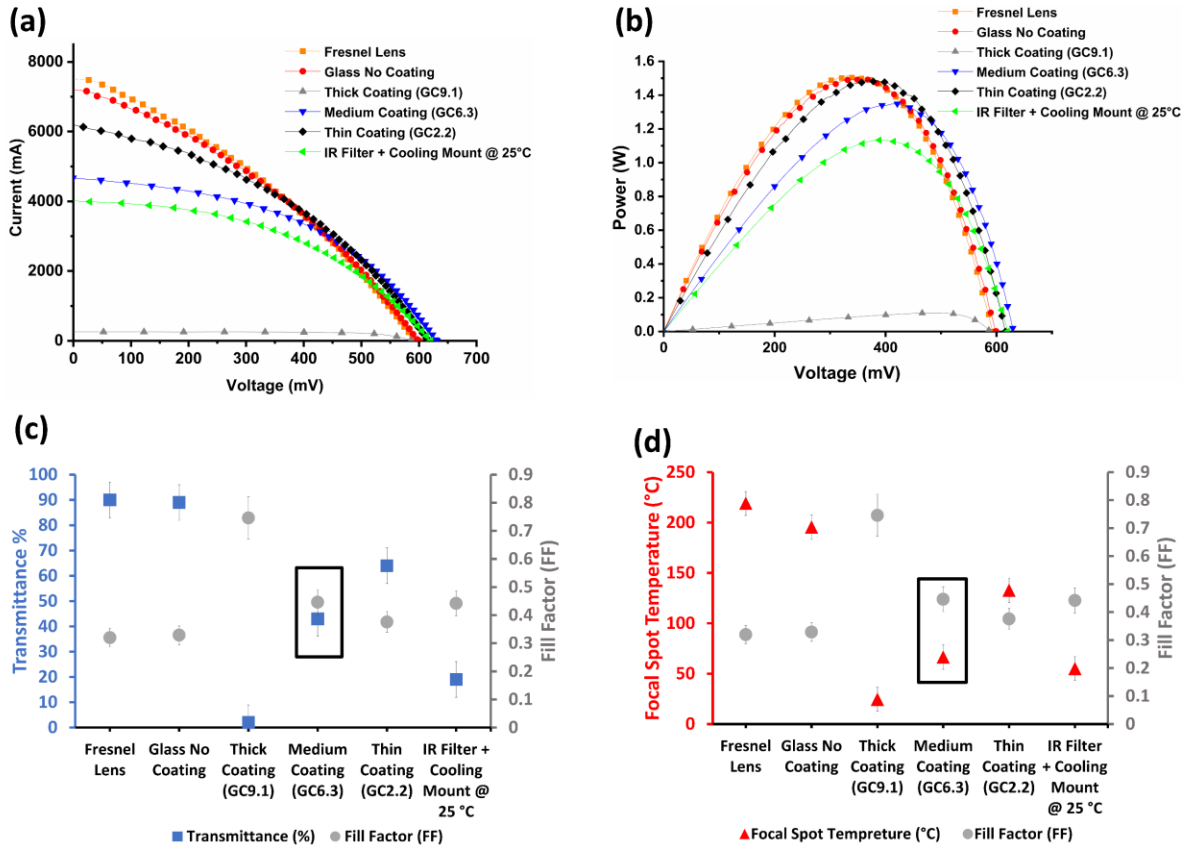

Fig. 9 (a) I-V curve and (b) power curve for polycrystalline Si solar cell, with glass, with adding different coating thickness, and with IR filter, respectively. (c) the inverse correlation between fill factor as a component of power quality and transmittance with a highlight box for the optimum performance ($GC_{6.3}$). (d) the inverse correlation between fill factor as a component of power quality and focal spot temperature with a highlight box for the optimum performance ($GC_{6.3}$).

Table 2 summarizes the results for the four different characterization approaches. The results confirmed that graphene is an appropriate material for natural density filter with optimum performance for the $GC_{6.3}$ as highlighted. Although the IR filter with a cooling mount

base showed the lowest focal spot temperature of 55°C and relatively similar FF value with $GC_{6.3}$; however, that is at the price of system weight, cost, and parasitic load. For the case of the IR filter associated with the cooling mount base, the focal spot temperature is given via considering the equilibrium temperature of 25°C for the cooling mount base and a 117.28°C for the focal spot temperature after the IR filter, which results in a focal spot temperature of 55°C. Also, the IR filter has shown a lower power output in comparison to $GC_{6.3}$ because $GC_{6.3}$ attenuates the intensity of solar irradiance across the wavelength range where the IR filter blocks all wavelengths beyond visible light with less control on the focal spot temperature. The optimization for the graphene thickness coating still has the potential to improve the overall performance further.

Graphene Neutral density (ND) filter	Chemical Characterization	Optical Characterization				Thermal Characterization	Electrical Characterization	
	Graphene thickness (µm)	Total transmittance (%T)	OD	Optical Efficiency (%)	Optical Concentration ratio (suns)	Focal Spot Temperature (°C)	Power output (W)	Fill Factor (FF)
Fresnel Lens	-	90	**0.045**	**90**	**18**	219	1.5	0.32
IR filter + cooling Mount @ 25 °C	-	19	**0.72**	**18**	**4**	55	1.13	0.442
Glass No Coating	-	89	**0.05**	**80**	**16**	196	1.49	0.329
Thick Coating ($GC_{9.1}$)	9.1 ± 0.05	2	1.69	**2**	**1**	24.6	0.11	0.746
Medium Coating ($GC_{6.3}$)	6.3 ± 0.1	43	0.36	**42**	**8**	66.4	1.34	0.446
Thin Coating ($GC_{2.2}$)	2.2 ± 0.2	64	0.19	**58**	**12**	132.7	1.49	0.376

Table 2 the summary for the characterization results for Graphene neutral density (ND) filter.

4. Graphene layer validation and cost analysis

To validate that the improvement in power output is predominantly due to the graphene layer, we have attenuated the solar simulator (WACOM) lamp intensity (helicon value) to examine the polycrystalline silicon (Si) solar cells at different solar irradiance value in the range of 1000-400W/m^2 in an interval of 100W/m^2 without GCs. This attenuation of input solar irradiance to the concentrator optic (Fresnel lens) results in a lower concentration ratio in the focal spot area which could be the reason for increasing the fill factor and hence the cell efficiency without GCs. Fig. 10a shows the downward slope of the cell efficiency from 5.96% to 2.44% with increasing the effective solar irradiance on the focal spot area for solar irradiance from 400W/m^2 to 1000W/m^2 corresponding for optical concentration ratio range from 7suns to 18suns. The $GC_{6.3}$ and $GC_{2.2}$ show a cell efficiency of 6.57% at 8suns and 4.91% at 13suns with effective solar irradiance on the focal spot at 1000W/m^2, respectively. The relatively low cell efficiency to the maximum cell efficiency of 17%[60] as reported by the manufacturer is simply due to using the single-junction solar cell beyond its design concentration range (1sun). Still, this utilization was important to see the temperature and concentration ratio reduction effects. The closest optical concentration ratio for the $GC_{6.3}$ at 8suns is the base case at 400W/m^2 with an optical concentration ratio of 7suns but with less efficiency by 12%, where the closest optical concentration ratio for the $GC_{2.2}$ is the base case at 700 W/m^2 with an optical concentration ratio of 12.8suns but with less efficiency by 28%. This comparison has certainly approved that the cell efficiency has been improved due to the integration of graphene as ND filter instead of lowering the concentration ratio. Thus, the same benefits should be in theory, replicable for a multijunction solar cell under ultrahigh concentration ratios. The $GC_{6.3}$ represent the highest cell efficiency. The GC challenges the optical efficiency of the CPV unit with improving cell efficiency in case of both $GC_{6.3}$ and $GC_{2.2}$. For $GC_{9.3,}$ the drop in the solar cell series-resistance is acquired by the highest drop in temperature resulting in FF of 0.746.

However, the power output of $GC_{9.3}$ is constrained as to counterbalance the extreme loss in optical efficiency. The cell efficiency improvements are simply due to the reduction in the high-series resistance polycrystalline Si solar cells caused by the thermo-optic absorption properties of GC

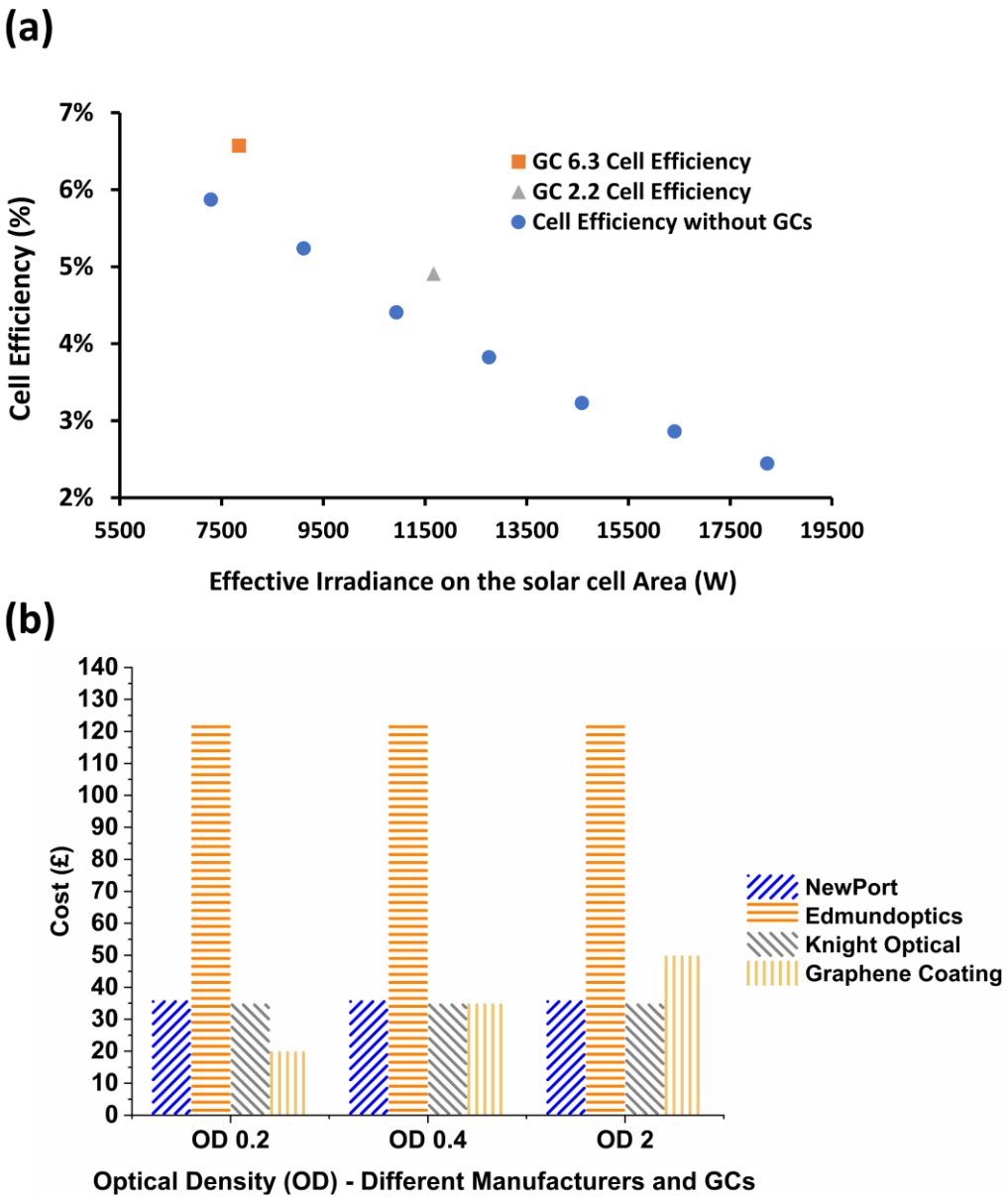

Fig. 10 (a) the cell efficiency verses the effective solar irradiance on the focal spot. (b) the cost of the developed GCs in comparison with the commercially available ND filters (Newport[50], Edmundoptics[51], and Knight optical[52]) for relatively similar optical density (OD).

The utilization of graphene as the ND filter has shown graphene as an excellent thermal filtering material. ND filters are commercially available by coating an absorptive material on low-iron glass, borosilicate glass, or fused silica with different thicknesses and design tolerance from one manufacturer to another to attenuate the light evenly across a spectral band. The simple concept to perform an ND filter is to have a coating thickness of not less than 2µm, and that was the case of not having GC samples less than 2.2µm. The ND filters are classified commercially based on their OD. According to the optical characterization, we have collected the cost for ND filters with comparable OD value to the GCs ones in this study from Newport, Edmund optics, and Knight optical. The cost of graphene coating was estimated considering only the low-iron glass and graphene ink, as in equation 3.

$$\boldsymbol{Grapahen\ coating} = \left(\frac{£15}{ml} \times \frac{3ml}{Thick\ Coating}\ or \frac{2ml}{Medium\ coating}\ or \frac{1ml}{Thin\ Coating}\right) + \frac{£5}{low\ iron\ glass\ (5cm \times 5cm)} \quad (3)$$

Fig. 10b shows the economic feasibility of $GC_{9.3}$, $GC_{6.1}$, and $GC_{2.2}$ in comparison with the available commercial options. The results show that the cost of the GCs is dependent on the OD (graphene thickness) where the cost of the other manufacturers is not affected by the degree of light transmittance. Indeed, the GCs are economically feasible in comparison with all ND filters manufactured by Edmundoptics and others with OD $\leq$ 0.4. In this study, the economic advantage of integrating graphene as the ND filter is to improve the CPV system power output where that occurs at OD $\leq$ 0.4. As highlighted previously, the medium coating (OD 0.36) is the optimum scenario for power output with still high potential for improvement. This improvement could be achieved by minimizing the amount of graphene by a certain percentage across the glass surface for more power output or by only coating a glass surface area comparable to the focal spot area which will result in a relative drop in the GC cost.

5. Conclusion

We have developed three graphene ND filters to attenuate the concentration of solar rays for a CPV system. To fabricate and characterize the ND filter, four different approaches such as chemical, optical, thermal and electrical characterizations have been adopted for a comprehensive understanding of the filter. All four characterization approaches have confirmed that the performance is dependent on the graphene thickness. The indoor experiment has been conducted for a polycrystalline Si solar cell, which is vulnerable to the observed level of temperature generated by SOG Fresnel lens (a geometrical concentration ratio of ≈20suns). The results have manifested graphene can bring into play as an ND filter component for a pre-illumination passive cooling mechanism. The simplistic employment of GC as an ND filter component can eliminate the traditional and strenuous cooling techniques such as active water cooling and combined heat pipe and sink cooling for CPV. Although the optimization of the GC thickness still has the potential to improve the overall performance further. The future direction of GC technology can pave the way on developing facile cooling methods to maintain the solar cell temperature low and stable for a CPV system.

Declaration of competing interest

The authors declare that they have no known competing financial interests or personal relationships that could have appeared to influence the work reported in this article.

Acknowledgment

M.A would like to duly acknowledge the financial support from the Saudi Arabia Culture Bureau in the U.K. A.R. and S.S. acknowledges Agri-tech Cornwall and the Isles of Scilly project (award number: 05R16P00366). The funders have no role in study design data collection, or preparation of the manuscript.

Reference

[1] M. Bercx, R. Saniz, B. Partoens, D. Lamoen, Exceeding the Shockley–Queisser Limit Within the Detailed Balance Framework, in: Many-Body Approaches at Different Scales, Springer International Publishing, Cham, 2018: pp. 177–184. doi:10.1007/978-3-319-72374-7_15.

[2] National Renewable Energy Laboratory (2020), Best Research-Cell Efficiencies. (2020). https://www.nrel.gov/pv/cell-efficiency.html.

[3] L.C. Herst, N. Ekins-Daukes, Fundamental losses in solar cells, Progress in Photovoltaics: Research and Applications. 19 (2010) 286–293. doi:10.1002/pip.

[4] J.G. Ingersoll, Simplified calculation of solar cell temperatures in terrestrial photovoltaic arrays, Journal of Solar Energy Engineering, Transactions of the ASME. 108 (1986) 95–101. doi:10.1115/1.3268087.

[5] M.W. Davis, A.H. Fanney, B.P. Dougherty, Prediction of building integrated photovoltaic cell temperatures, Journal of Solar Energy Engineering, Transactions of the ASME. 123 (2001) 200–210. doi:10.1115/1.1385825.

[6] A.D. Jones, C.P. Underwood, A thermal model for photovoltaic systems, Fuel and Energy Abstracts. 43 (2002) 199. doi:10.1016/s0140-6701(02)85831-3.

[7] M. Cui, N. Chen, X. Yang, Y. Wang, Y. Bai, X. Zhang, Thermal analysis and test for single concentrator solar cells, Journal of Semiconductors. 30 (2009). doi:10.1088/1674-4926/30/4/044011.

[8] O.Z. Sharaf, M.F. Orhann, Concentrated photovoltaic thermal (CPVT) solar collector systems: Part II - Implemented systems, performance assessment, and future directions, Renewable and Sustainable Energy Reviews. 50 (2015) 1566–1633. doi:10.1016/j.rser.2014.07.215.

[9] O.Z. Sharaf, M.F. Orhan, Concentrated photovoltaic thermal (CPVT) solar collector systems: Part I - Fundamentals, design considerations and current technologies, Renewable and Sustainable Energy Reviews. 50 (2015) 1500–1565. doi:10.1016/j.rser.2015.05.036.

[10] P. Dwivedi, K. Sudhakar, A. Soni, E. Solomin, I. Kirpichnikova, Advanced cooling techniques of P.V. modules: A state of art, Case Studies in Thermal Engineering. 21 (2020) 100674. doi:10.1016/j.csite.2020.100674.

[11] A. Royne, C.J. Dey, D.R. Mills, Cooling of photovoltaic cells under concentrated illumination: A critical review, Solar Energy Materials and Solar Cells. 86 (2005) 451–483. doi:10.1016/j.solmat.2004.09.003.

[12] L. Micheli, N. Sarmah, X. Luo, K.S. Reddy, T.K. Mallick, Opportunities and challenges in micro- and nano-technologies for concentrating photovoltaic cooling : A review, Renewable and Sustainable Energy Reviews. 20 (2013) 595–610. doi:10.1016/j.rser.2012.11.051.

[13] L. Micheli, K.S. Reddy, T.K. Mallick, General correlations among geometry, orientation

and thermal performance of natural convective micro-finned heat sinks, International Journal of Heat and Mass Transfer. 91 (2015) 711–724. doi:10.1016/j.ijheatmasstransfer.2015.08.015.

[14] L. Micheli, N. Sarmah, E.F. Fernandez, K.S. Reddy, T.K. Mallick, Technical issues and challenges in the fabrication of a 144-Cell 500× Concentrating Photovoltaic receiver, 2014 IEEE 40th Photovoltaic Specialist Conference, PVSC 2014. (2014) 2921–2925. doi:10.1109/PVSC.2014.6925543.

[15] E.M. Abo-Zahhad, S. Ookawara, A. Radwan, A.H. El-Shazly, M.F. Elkady, Numerical analyses of hybrid jet impingement/microchannel cooling device for thermal management of high concentrator triple-junction solar cell, Applied Energy. 253 (2019) 113538. doi:10.1016/j.apenergy.2019.113538.

[16] E.M. Abo-Zahhad, S. Ookawara, A. Radwan, A.H. El-Shazly, M.F. El-Kady, M.F.C. Esmail, Performance, limits, and thermal stress analysis of high concentrator multijunction solar cell under passive cooling conditions, Applied Thermal Engineering. 164 (2020) 114497. doi:10.1016/j.applthermaleng.2019.114497.

[17] M. Alzahrani, H. Baig, K. Shanks, T. Mallick, Estimation of the performance limits of a concentrator solar cell coupled with a micro heat sink based on a finite element simulation, Applied Thermal Engineering. (2020) 115315. doi:10.1016/j.applthermaleng.2020.115315.

[18] A. Aldossary, S. Mahmoud, R. Al-dadah, Technical feasibility study of passive and active cooling for concentrator PV in harsh environment, Applied Thermal Engineering. 100 (2016) 490–500. doi:10.1016/j.applthermaleng.2016.02.023.

[19] Y.L. He, K. Wang, Y. Qiu, B.C. Du, Q. Liang, S. Du, Review of the solar flux distribution in concentrated solar power: Non-uniform features, challenges, and solutions, Applied Thermal Engineering. 149 (2019) 448–474. doi:10.1016/j.applthermaleng.2018.12.006.

[20] Y.L. He, K. Wang, Y. Qiu, B.C. Du, Q. Liang, S. Du, Review of the solar flux distribution in concentrated solar power: Non-uniform features, challenges, and solutions, Elsevier Ltd, 2019. doi:10.1016/j.applthermaleng.2018.12.006.

[21] S. Wang, J. Shi, H.H. Chen, S.R. Schafer, M. Munir, G. Stecker, W. Pan, J.J. Lee, C.L. Chen, Cooling design and evaluation for photovoltaic cells within constrained space in a CPV/CSP hybrid solar system, Applied Thermal Engineering. 110 (2017) 369–381. doi:10.1016/j.applthermaleng.2016.08.196.

[22] M. Renzi, L. Egidi, G. Comodi, Performance analysis of two 3.5 kWp CPV systems under real operating conditions, Applied Energy. 160 (2015) 687–696. doi:10.1016/j.apenergy.2015.08.096.

[23] A. Mojiri, R. Taylor, E. Thomsen, G. Rosengarten, Spectral beam splitting for ef fi cient conversion of solar energy — A review, Renewable and Sustainable Energy Reviews. 28 (2013) 654–663. doi:10.1016/j.rser.2013.08.026.

[24] S.-L. Jiang, P. Hu, S.-P. Mo, Z.-S. Chen, Modeling for Two-Stage Dish Concentrating Spectral Beam Splitting Photovoltaic/Thermal System, in: 2009 Asia-Pacific Power and

Energy Engineering Conference, IEEE, 2009: pp. 1–4. doi:10.1109/APPEEC.2009.4918499.

[25] X. Ju, C. Xu, X. Han, X. Du, G. Wei, Y. Yang, A review of the concentrated photovoltaic/thermal (CPVT) hybrid solar systems based on the spectral beam splitting technology, Applied Energy. 187 (2017) 534–563. doi:10.1016/j.apenergy.2016.11.087.

[26] C. Kandilli, Performance analysis of a novel concentrating photovoltaic combined system, Energy Conversion and Management. 67 (2013) 186–196. doi:10.1016/j.enconman.2012.11.020.

[27] A. Kumar, N. Deo, H.L. Yadav, Analysis of design parameters for wavelength selective holographic solar concentrators, Conference Record of the IEEE Photovoltaic Specialists Conference. (2008) 8–11. doi:10.1109/PVSC.2008.4922898.

[28] W.G.J.H.M. van Sark, Luminescent solar concentrators - A low cost photovoltaics alternative, Renewable Energy. 49 (2013) 207–210. doi:10.1016/j.renene.2012.01.030.

[29] D. Mattox, R. Sowell, A SURVEY OF SELECTIVE SOLAR ABSORBERS AND THEIR LIMITATIONS, JOURNAL DE PHYSIQUE. (1981). doi:1981102ff. ffjpa-00220652.

[30] A. Boubault, C.K. Ho, A. Hall, T.N. Lambert, A. Ambrosini, Durability of solar absorber coatings and their cost-effectiveness, Solar Energy Materials and Solar Cells. 166 (2017) 176–184. doi:10.1016/j.solmat.2017.03.010.

[31] K. Xu, M. Du, L. Hao, J. Mi, Q. Yu, S. Li, A review of high-temperature selective absorbing coatings for solar thermal applications, Journal of Materiomics. 6 (2020) 167–182. doi:10.1016/j.jmat.2019.12.012.

[32] A. Roy, A. Ghosh, D. Benson, T.K. Mallick, S. Sundaram, Emplacement of screen-printed graphene oxide coating for building thermal comfort discernment, Scientific Reports. 10 (2020) 15578. doi:10.1038/s41598-020-72670-8.

[33] V. Dhinakaran, M. Lavanya, K. Vigneswari, M. Ravichandran, M.D. Vijayakumar, Review on exploration of graphene in diverse applications and its future horizon, Materials Today: Proceedings. (2020). doi:10.1016/j.matpr.2019.12.369.

[34] T.C. Dinadayalane, J. Leszczynski, Remarkable diversity of carbon-carbon bonds: Structures and properties of fullerenes, carbon nanotubes, and graphene, Structural Chemistry. 21 (2010) 1155–1169. doi:10.1007/s11224-010-9670-2.

[35] M.J. Allen, V.C. Tung, R.B. Kaner, Honeycomb carbon: A review of graphene, Chemical Reviews. 110 (2010) 132–145. doi:10.1021/cr900070d.

[36] X. Yu, H. Cheng, M. Zhang, Y. Zhao, L. Qu, G. Shi, Graphene-based smart materials, Nature Reviews Materials. 2 (2017) 17046. doi:10.1038/natrevmats.2017.46.

[37] H.S. Ahn, J.M. Kim, T. Kim, S.C. Park, J.M. Kim, Y. Park, D.I. Yu, K.W. Hwang, H. Jo, H.S. Park, H. Kim, M.H. Kim, Enhanced heat transfer is dependent on thickness of graphene films: the heat dissipation during boiling, Scientific Reports. 4 (2015) 6276. doi:10.1038/srep06276.

[38] V.-D. Dao, H.-S. Choi, Carbon-Based Sunlight Absorbers in Solar-Driven Steam Generation Devices, Global Challenges. 2 (2018) 1700094. doi:10.1002/gch2.201700094.

[39] M. Gao, L. Zhu, C.K. Peh, G.W. Ho, Solar absorber material and system designs for photothermal water vaporization towards clean water and energy production, Energy & Environmental Science. 12 (2019) 841–864. doi:10.1039/C8EE01146J.

[40] H. Atwater, A. Polman, E. Kosten, D. Callahan, P. Spinelli, C. Eisler, M. Escarra, E. Warmann, C. Flowers, Nanophotonic design principles for ultrahigh efficiency photovoltaics, AIP Conference Proceedings. 1519 (2013) 17–21. doi:10.1063/1.4794700.

[41] J.P. Ferrer-Rodríguez, E.F. Fernández, F. Almonacid, P. Pérez-Higueras, Optical design of a 4-off-axis-unit Cassegrain ultra-high concentrator photovoltaics module with a central receiver, Optics Letters. 41 (2016) 1985. doi:10.1364/ol.41.001985.

[42] C. Algora, I. Rey-Stolle, Chapter 2 The Interest and Potential of Ultra-High Concentration. Next Generation of Photovoltaics: New Concept, Springer Berlin Heidelberg, Berlin, Heidelberg, 2012. doi:10.1007/978-3-642-23369-2.

[43] K. Shanks, J.P. Ferrer-rodriguez, E.F. Fernández, F. Almonacid, A > 3000 suns high concentrator photovoltaic design based on multiple Fresnel lens primaries focusing to one central solar cell, Solar Energy. 169 (2018) 457–467. doi:10.1016/j.solener.2018.05.016.

[44] M. Data, T. Average, E. Data, Concentrator Triple Junction Solar Cell Cell Type : 3C44C-3 × 3 mm2 Azur Space, (2012) 3–6. http://www.azurspace.com/images/products/0004357-00-01_3C44_AzurDesign_3x3.pdf.

[45] X. Ding, X. Yang, J. Wang, K. Guo, F. Shen, H. Zhou, R. Sun, Z. Ding, J. Gao, Z. Guo, Theoretical analysis and simulation of a tunable mid-infrared filter based on Ge2Sb2Te5 (GST) metasurface, Superlattices and Microstructures. 132 (2019) 106169. doi:10.1016/j.spmi.2019.106169.

[46] A. Emadi, H. Wu, G. De Graaf, R.F. Wolffenbuttel, IR microspectrometers based on linear-variable optical filters, Procedia Engineering. 25 (2011) 1401–1404. doi:10.1016/j.proeng.2011.12.346.

[47] K. Xu, M. Du, L. Hao, J. Mi, Q. Yu, S. Li, A review of high-temperature selective absorbing coatings for solar thermal applications, Journal of Materiomics. 6 (2020) 167–182. doi:10.1016/j.jmat.2019.12.012.

[48] W. Li, Y. Shi, K. Chen, L. Zhu, S. Fan, A Comprehensive Photonic Approach for Solar Cell Cooling, ACS Photonics. 4 (2017) 774–782. doi:10.1021/acsphotonics.7b00089.

[49] G.K. Dalapati, S. Masudy-Panah, S.T. Chua, M. Sharma, T.I. Wong, H.R. Tan, D. Chi, Color tunable low cost transparent heat reflector using copper and titanium oxide for energy saving application, Scientific Reports. 6 (2016) 1–14. doi:10.1038/srep20182.

[50] Newport Corporation, Neutral Density Filter Selection Guide, (n.d.). https://www.newport.com/g/neutral-density-filter-selection-guide (accessed March

1, 2020).

[51] EO Edmund Optics Worldwide, Neutral Density (ND) Filters, (n.d.). https://www.edmundoptics.com/c/neutral-density-filters/619/# (accessed March 1, 2020).

[52] KO KNIGHT OPTICAL, Metallic neutral density filters, (n.d.). https://www.knightoptical.com/stock/optical-components/uvvisnir-optics/filters/neutral-density-filters/metallic-neutral-density-filters/ (accessed March 1, 2020).

[53] H.A. Kazem, M.T. Chaichan, The Impact of Using Solar Colored Filters to Cover the PV Panel in Its Outcomes, Scholars Bulletin. 2 (2016) 464–469. doi:10.21276/sb.2016.2.7.5.

[54] B. Ramkiran, C.K. Sundarabalan, K. Sudhakar, Performance evaluation of solar PV module with filters in an outdoor environment, Case Studies in Thermal Engineering. 21 (2020) 100700. doi:10.1016/j.csite.2020.100700.

[55] L. Barrutia, C. Algora, I. Rey-Stolle, OPTIMIZATION PATHWAYS TO IMPROVE GaInP/GaInAs/Ge TRIPLE JUNCTION SOLAR CELLS FOR CPV APPLICATIONS, Universidad Politécnica de Madri, 2017.

[56] L. Barrutia, I. Lombardero, M. Ochoa, M. Gabás, I. García, T. Palacios, A. Johnson, I. Rey-Stolle, C. Algora, On the use of graphene to improve the performance of concentrator III-V multijunction solar cells, Progress in Photovoltaics: Research and Applications. 28 (2020) 60–70. doi:10.1002/pip.3207.

[57] I. Rey-Stolle, L. Barrutia, I. García, C. Algora, Assessment of the energy yield gain in high CPV systems using graphene-enhanced III-V multijunction solar cells, AIP Conference Proceedings. 2149 (2019). doi:10.1063/1.5124173.

[58] K. Shanks, S. Senthilarasu, T.K. Mallick, Optics for concentrating photovoltaics: Trends, limits and opportunities for materials and design, Renewable and Sustainable Energy Reviews. 60 (2016) 394–407. doi:10.1016/j.rser.2016.01.089.

[59] H. Baig, N. Sellami, D. Chemisana, J. Rosell, T.K. Mallick, Performance analysis of a dielectric based 3D building integrated concentrating photovoltaic system, Solar Energy. 103 (2014) 525–540. doi:10.1016/j.solener.2014.03.002.

[60] A. Ahmed, M. Alzahrani, K. Shanks, S. Sundaram, T.K. Mallick, Effect of using an infrared filter on the performance of a silicon solar cell for an ultra-high concentrator photovoltaic system, Materials Letters. 277 (2020) 128332. doi:10.1016/j.matlet.2020.128332.